Hydration force and dynamic squeeze-out of hydration water under subnanometer confinement

2008 J. Phys.: Condens. Matter 20 354017

(http://iopscience.iop.org/0953-8984/20/35/354017)

IOP Publishing Journal of Physics: Condensed Matter

J. Phys.: Condens. Matter **20** (2008) 354017 (8pp) doi:10.1088/0953-8984/20/35/354017

Hydration force and dynamic squeeze-out of hydration water under subnanometer confinement

Yongsheng Leng[1]

Department of Chemical Engineering, Vanderbilt University, Nashville, TN 37235, USA

E-mail: yongsheng.leng@vanderbilt.edu

Received 29 January 2008, in final form 26 February 2008
Published 11 August 2008
Online at stacks.iop.org/JPhysCM/20/354017

Abstract

We have performed molecular dynamics simulations to study the normal forces between two mica surfaces in water and the consequent dynamic squeeze-out process. A liquid–vapor molecular ensemble has been designed for this purpose. We find, however, that only the two-layer hydration water can support a repulsive hydration force, and beyond this thickness the overall forces are attractive. From the hydrodynamic pressure developed during a normal approach and dynamic squeeze-out, we estimate that the viscosity of confined hydration water in the thickness of 0.7–1.35 nm is about 5–16 times the bulk value. A steered diffusion model has been proposed, which directly predicts the critical velocity below which hydrodynamic effects can be eliminated in hydration force measurements.

(Some figures in this article are in colour only in the electronic version)

1. Introduction

The nature of water confined between charged surfaces at nanometer distances is an important fundamental issue and has many implications in materials science and biological processes, such as the stability of colloidal dispersion, adhesion and wetting in nanoscale machines, the interactions between biomembranes, and water transport through ion channels and through crowded intracellular environment. In surface force measurements [1], it is well known that when the distance between two charged mica surfaces in a high-concentration salt solution is within a few nanometers or less, very strong repulsive hydration forces will develop. These short-range hydration forces deviate significantly from the continuum double-layer interactions—the Derjaguin–Landau–Verwey–Overbeek (DLVO) theory [2, 3]. Measurement of hydration force using surface force apparatus (SFA) was first accomplished by Israelachvili and Adam [4], and later by Pashley [5, 6]. Recent surface force balance (SFB) experiments by Raviv and Klein [7, 8] further revealed the very fluidic nature of water even under subnanometer confinement. The origin and nature of this hydration force has long been controversial, and explanations appear to be related to the central role of hydrated metal ions [1, 5, 6, 8, 9]. This is particularly in contrast to the situation in which the freshly cleaved mica sheets are immersed in dilute or acid solutions, no repulsive hydration forces are observed [5]. This scenario has been attributed to the fact that the potassium ions (K^+) that originally bind on the negatively charged sites on mica surfaces are exchanged with protons (in the form of H_3O^+). It was speculated [6, 9] that the penetration of protons into the mica lattice leads to a strong jump-in adhesive contact between the two surfaces, due to the long-range van der Waals attraction in water [7].

We are concerned with the development of a molecular dynamics (MD) simulation approach to explore the repulsive hydration force mechanism, and the related dynamic squeeze-out behavior of water confined between two mica surfaces. For the squeeze-out behavior of non-polar liquids confined between solid surfaces, substantial work has been done in which deformation of solid substrate was considered and the void nucleation model was applied [10, 11]. For soft aqueous systems, our primary concern focuses on the dynamic squeeze-out properties of hydration water, thus, the effect of mica crystal deformation has been omitted. A fundamental question that needs to be answered is, in pure water with potassium

[1] Present address: Department of Mechanical and Aerospace Engineering, The George Washington University, Washington, DC 20052, USA.

ions being attached to mica surfaces, at what distance will the repulsive hydration force develop? This scenario may correspond to the case in which the mica sheets are immersed in a high-concentration salt solution under extreme confinement (ca 1 nm), where only counterions survive in mica slit pores to balance the negatively charged sites [8]. In the following sections, we will first describe a liquid–vapor (L–V) molecular ensemble that allows a water droplet to be freely squeezed-out during a normal approach between two mica surfaces. One of the advantages of using an L–V molecular ensemble is that we can circumvent the difficulty of pressure tensor calculations, and simultaneously, avoid scaling particle coordinates to control the pressure in the isothermal–isobaric (*NPT*) ensemble. We then use the L–V ensemble to simulate the normal approach of mica and dynamic squeeze-out of water, beginning from a relatively larger distance. We find that when the hydrated K^+ ions are attached to mica surfaces the overall forces between mica surfaces are *attractive* for three hydration layers and above. A very strong *repulsive* hydration force is observed only at the last two-layer hydration water ($H = 0.6$–0.7 nm). Further investigations demonstrate that the observed repulsive forces are rate-dependent, suggesting that hydrodynamics is the main effect. From the hydrodynamic pressures calculated we estimate that the viscosity of the hydration layer under subnanometer confinement is about 5–16 times the bulk value, less than what we obtained previously [12, 13]. Through a 'steered diffusion' model, we predict that in surface force measurements where the contact radii are typically around a few μm, the normal approach speed *without* hydrodynamic effect, particularly at subnanometer distance, should be sufficiently slow.

2. Simulation methodology—the liquid–vapor (L–V) molecular ensemble

Liquid film confined between two solid surfaces is a strongly inhomogeneous system. The pressures parallel to the confining walls may differ considerably from the normal pressure due to the formation of layered structure of confined film and the related solvation effect. In surface force experiments, the equilibrium between the confined and the bulk fluids requires that the chemical potentials in these two regions should be equal. One way to represent the connection between the confined and bulk fluids is to use the so-called isothermal–isostress ensemble, in which the lateral pressures are controlled to the desired bulk values [14]. A grand canonical molecular dynamics (GCMD) approach was also designed for this purpose [15]. However, for a two-dimensional (2D) confined system, particularly when explicit surface atoms and charges are present, the calculation of the pressure tensor is a nontrivial issue. Since the pressure is only meaningful to the confined fluid, the treatment of long-range electrostatic contributions to the pressure tensor will be very difficult for this inhomogeneous system. Although the Ewald summation [16] technique can be used to calculate the electrostatic interaction forces for all the MD particles, the extraction of contributions of these forces to the pressure tensor on the fluid particles is not straightforward. Another issue is related to the scaling of particle coordinates in the pressure control. When the simulation box becomes quite elongated, as we will see in this study, scaling particle coordinates and box lengths may generate waves that eventually result in artificial oscillations in force profiles (see the appendix for a detailed case study).

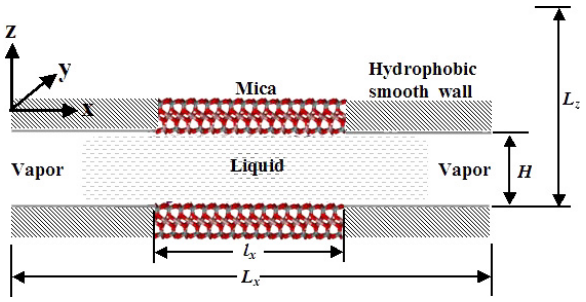

Figure 1. Illustration of a liquid–vapor (L–V) molecular ensemble. The two mica surfaces are smoothly connected to frictionless hydrophobic walls to accommodate the squeezed-out water molecules during normal approach.

We note that in surface force experiments, the ambient condition requires that the bulk liquid pressure should be equal to 1 atm ($= 0.9869 \times 10^5$ Pa). This is a vanishingly low pressure compared to the thermal fluctuations of internal pressures in liquids. For this reason, instead of controlling the lateral pressure by scaling the particle coordinates and simulation box lengths, we leave this variable as an uncontrolled one by introducing two vapor phases around the confined liquid phase. The sketch of this liquid–vapor (L–V) molecular ensemble is shown in figure 1. A recent study [17] for different water models showed that at $T = 300$ K the L–V interface is quite stable and the normal pressure at this interface is around zero.

The molecular system consists of a water droplet that contains 1152 TIP4P [18] water molecules, two mica clay surfaces (the chemical formula for one unit cell of muscovite mica is $K_2Al_4(Al, Si_3)_2O_{20}(OH)_4$) [19], and movable K^+ ions that balance the negatively charged tetrahedral sites due to the substitution of Al for Si in the tetrahedral sheets. Each mica surface contains 8×4 unit cells (the lengths of unit cell are $a = 0.5194$ and $b = 0.9015$ nm), thus the dimensions of mica plate in the x- and y- directions are $l_x = 4.155$ and $l_y = 3.606$ nm, respectively, and there are, in total, thirty-two potassium ions attached to each mica surface. Atomic interaction potentials involving mica, water, and potassium ions are derived from Boek *et al*'s force field for clay minerals [20]. To allow for the water droplet to be freely squeezed-out during normal approach, the mica slit pore is smoothly connected to two frictionless hydrophobic pores along the x-direction, as shown in figure 1. The hydrophobic confining walls only apply a 9-3 Lennard-Jones surface potential [21] to the water molecules in the normal direction. Periodic boundary conditions are applied in three dimensions. The simulation box length in the x-direction, L_x, is sufficiently large to maintain a stable liquid–vapor interface that prevents the water droplet from being collapsed with its images. Here, we select $L_x = 30$–40 nm. The simulation box lengths in the y- and z-directions are

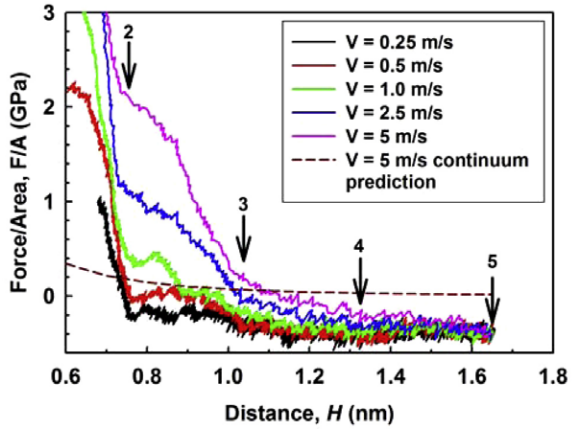

Figure 2. The normal force/area profiles between two mica surfaces in a water droplet at different normal approach speed. The rate-dependent behavior of normal forces comes from the hydrodynamic effect. For comparison, the continuum hydrodynamic pressure at $V = 5$ m s^{-1}, derived from the Reynolds equation for a rigid rectangular plate approaching a solid substrate in water is also shown in the figure. The numbers 2–5 indicate different layers of hydration water.

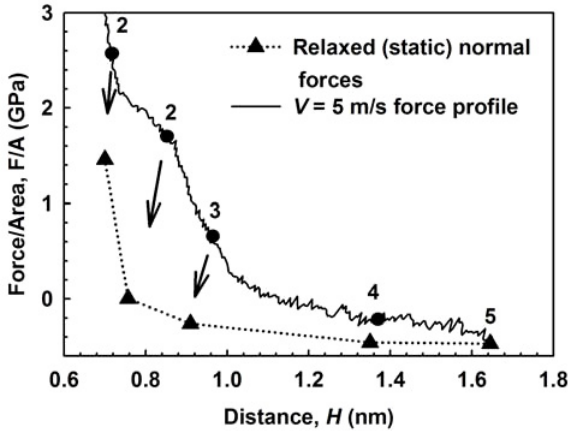

Figure 3. The relaxed static normal forces versus distances for the case of $V = 5$ m s^{-1} normal approach. It is seen that only two water layers can support a repulsive hydration force. The numbers 2–5 indicate different layers of hydration water. The arrows point to the relaxed pressures from dynamic to static equilibrium states.

$L_y = 3.606$ and $L_z = 5.0$ nm, respectively. This arrangement leads to a quite large number of reciprocal-space vectors (4800–6400) being needed to accurately calculate the Ewald summation [16] for the long-range electrostatic interactions.

3. Results

3.1. The normal force profiles

In simulating the normal approach and dynamic squeeze-out processes, we assume that the upper mica plate is connected to a driving stage through a normal spring ($k_z = 150$ N m^{-1}). The normal approach speed, V, of the driving stage varies from 0.25–5 m s^{-1}. The dynamic inertia of mica plate is selected to be $M = 2000$ oxygen mass $= 5.3 \times 10^{-20}$ g. These mechanical parameters in MD regime are dramatically different from those in surface force experiments [22] and have been extensively discussed previously [13]. The normal approach of the upper mica plate starts from an equilibrium molecular configuration at 298 K where the thickness, H, of the hydration layer is about 1.65 nm. We find that the liquid–vapor interface of the water droplet is quite stable, and the evaporation of a water molecule at room temperature is a rare event during simulation runs, consistent with other studies [17].

Figure 2 shows the normal force/area profiles between two mica surfaces in water at different approach speeds. Initially, all the forces at larger distances are attractive. We attribute this to three reasons [1]. First, for a system of charges that are electrically neutral the electrostatic contribution to the net force is attractive, favoring the association of the system. Second, the zero electric field between two negatively charged mica surfaces leads to the migration of K^+ ions towards both mica surfaces due to their mutual electric repulsion. The attachment of K^+ ions on mica surfaces results in a lack of osmotic pressure developing between mica surfaces. This osmotic pressure, if it exists, will force metal ions away from mica surfaces to increase configurational entropy [1]. Third, we have not yet considered extra counterions and anions in the molecular system that corresponds to the real situation in a dense electrolyte, which would favor the development of repulsive osmotic pressures. However, figure 2 does show that there is a rate-dependent behavior of the normal forces in the velocity window we studied in MD regime. At the highest approach speed ($V = 5$ m s^{-1}) repulsive force starts at a distance of $D \sim 1.1$ nm, whereas at the lowest speed ($V = 0.25$ m s^{-1}) the overall forces are attractive until the thickness of hydration layer is less than 0.75 nm (two hydration layers). Evidently, this rate-dependent phenomenon comes from a hydrodynamic effect that interferes the hydration forces. From the figure we see that the hydrodynamic forces from MD simulations are roughly proportional to the approach speed, V. A detailed hydrodynamics analysis will be given in the next section.

The next question is whether a *static* repulsive hydration force exists in the subnanometer regime between mica surfaces in water, with K^+ ions being attached to mica surfaces. In figure 3 we show the relaxed normal force/area values for the case of $V = 5$ m s^{-1} normal approach. These relaxed forces (marked by solid triangles in the figure) are obtained from the relaxations starting from different approaching stages (marked by solid circles, as well as the numbers of hydration water layers in the $V = 5$ m s^{-1} force profile). At each stage, the driving stage completely stops and the whole molecular system (including upper mica plate, water molecules and K^+ ions) is allowed to evolve with time. As expected, all the relaxed forces corresponding to 5, 4, and 3 hydration layers are attractive, and it is only in the 2-layer hydration water ($H = 0.7$–0.75 nm) that the confined film can support a repulsive normal load. Extensive MD runs at other different approach speeds ($V = 0.25$–2.5 m s^{-1}) also confirm that when static equilibrium is reached, all the force profiles shown in figure 2 collapse to the same relaxed force profile shown in

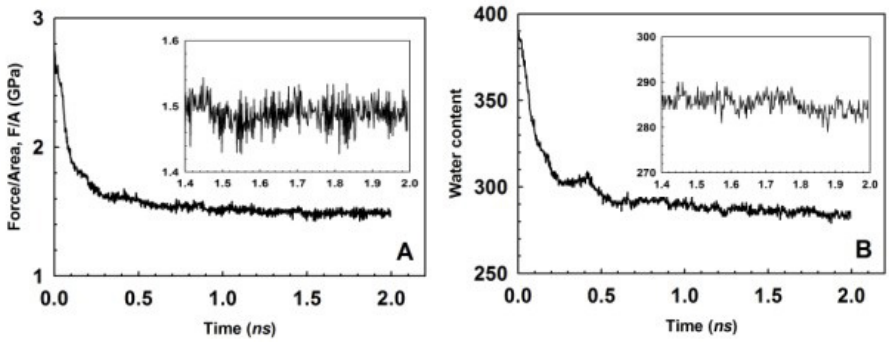

Figure 4. The relaxations of (A) normal force/area and (B) water content for the case of $V = 5$ m s^{-1} normal approach at the surface distance of $H = 0.7$ nm. The insets show the equilibrium fluctuations during the last 600 ps MD run.

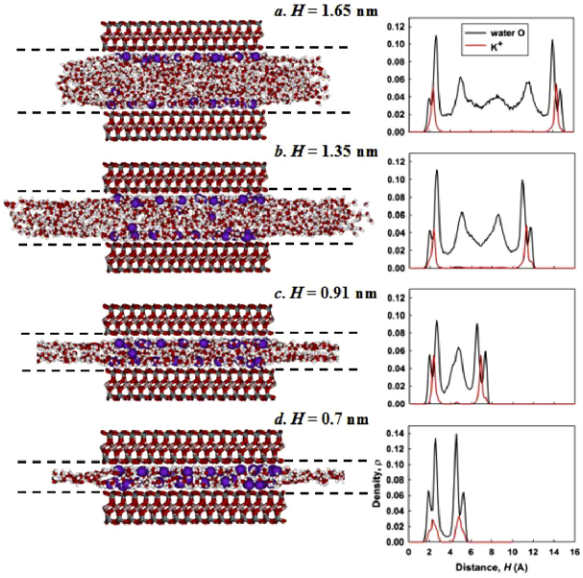

Figure 5. Equilibrium molecular configurations of different hydration layers and the corresponding water O and potassium ion (K^+) density distributions along the thickness (z-) direction. These density distributions were obtained from the time averages (at least 100 ps) in many bins along the z-direction. The dashed lines represent the hydrophobic surfaces that smoothly connect to the mica slit pore. Water depletion near hydrophobic walls is clearly shown.

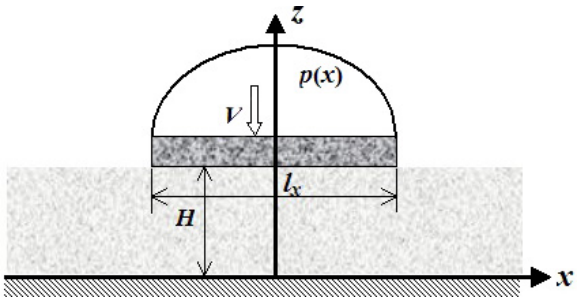

Figure 6. Hydrodynamics model of a rigid rectangular plate approaching a solid substrate in a medium. The cartoon shows a parabolic pressure distribution, $p(x)$, developed during the normal approach of the plate, as predicted by equation (2).

figure 3. The detailed relaxations of force/area and water content at the highest load (corresponding to $H = 0.7$ nm in figure 3) for the case of $V = 5$ m s^{-1} normal approach are shown in figure 4. Evidently, the ability of two-layer hydration water to support a large load (∼1.5 GPa) is convincing. During this ∼2 ns relaxation process the water content in the mica slit pore is reduced from 387 to roughly 284 water molecules.

Figure 5 shows the detailed static equilibrium molecular configurations of hydration layers, as well as the water O and K^+ ion density distributions. It is interesting to see that there is a slight depletion of water molecules in the hydrophobic zone due to the hydrophobic wall effects. Note that the non-zero valleys in water O density distributions, even for the $H = 0.7$ nm two-layer hydration water (figure 5(d)), indicate that water under subnanometer confinement still has a significant diffusion (see below). The adsorbed and the first hydration peaks of water are remarkable [23], whereas the hydrated potassium peak is located in between. The observation of repulsive pressure only at two hydration layers seems to imply that pure water, even though it can form diffused layers at larger distances, would not be able to support a normal load. It is only when the hydrated metal ions are present and the hydration shells of these metal ions begin to overlap (figure 5(d)) that the hydration layers can bear a positive load. In consequence, this seems to support such a fundamental idea: the load bearing capacity of bound hydration layers is due to the very strong hydration energy between water molecules and hydrated metal ions such that any further squeeze-out of a fraction of water molecules in the overlapped hydration shells will result in a large energy penalty (a large positive load) to dehydrate the bound counterions [5, 8].

3.2. The fluidity of water during dynamic squeeze-out

We now consider at very low Reynolds number ($N_R \ll 1$) the continuum hydrodynamic pressure developed when a rectangular rigid plate approaches an infinite solid substrate with a velocity, V, in a medium, as shown in figure 6. The thickness of the confined liquid film is H and its viscosity η is assumed to be constant across the film. The plate has a width of l_x in the x-direction and is sufficiently long in the y-direction. This is a classical problem of dynamic squeeze-out

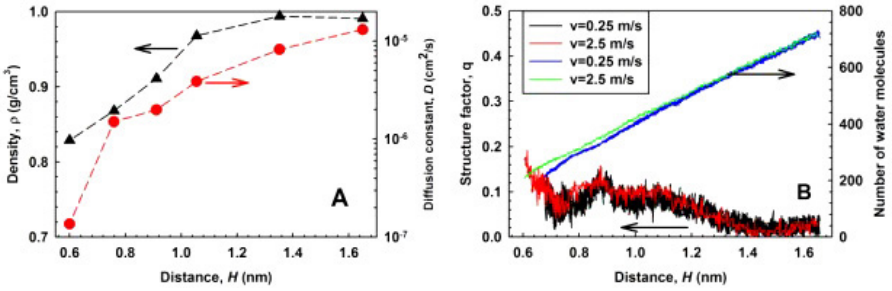

Figure 7. Dynamic squeeze-out of a water droplet. (A) Variations of water density and diffusion constant versus the distance between two mica surfaces. (B) Continuous decrease of water content and variations of structure factor of water molecules in the mica slit pore for $V = 0.25$ and 2.5 m s^{-1}.

in textbook fluid mechanics [24]. Starting from the Navier–Stokes equations to solve this problem seems inconvenient. An alternative way is to use the Reynolds equation in lubrication theory [25], assuming that the pressure across the liquid film is constant and the no-slip boundary condition holds. The general Reynolds equation for this dynamic process can be written as [25]

$$\frac{\partial}{\partial x}\left(H^3\frac{\partial p}{\partial x}\right)+\frac{\partial}{\partial y}\left(H^3\frac{\partial p}{\partial y}\right)=12\eta\frac{\partial H}{\partial t}. \qquad (1)$$

Since the geometry of the plate is invariant in the y-direction, the pressure p will only be a function of x. Note that when the plate is moving downwards with a velocity V, we have $\partial H/\partial t = -V$. The solution for the pressure p, with boundary conditions $p(x = \pm l_x/2) = 0$ and $\partial p/\partial x\ (x = 0) = 0$, is obtained as

$$p=\frac{6\eta V}{H^3}\left(\frac{l_x^2}{4}-x^2\right). \qquad (2)$$

This pressure distribution is parabolic along the x-direction, as shown in figure 6. The mean pressure over the plate width (l_x) is given by

$$\bar{p}=\frac{\eta V l_x^2}{H^3}. \qquad (3)$$

We see that the hydrodynamic pressure is proportional to V, as we have already seen in MD simulations in figure 2 (the magnitude of force profile is roughly proportional to V). In previous studies for a mica–water–ion system [13], we demonstrated that the no-slip boundary condition under shear still holds even when water is confined in a subnanometer gap. For the MD simulation system sketched in figure 1, we have calculated the Reynolds number at the highest approach speed ($V = 5$ m s^{-1}). Assuming the viscosity of water takes the bulk value ($\eta = \eta_{\rm bulk} = 0.86 \times 10^{-3}$ Pa s at 296 K), we have $N_{\rm R} = l_x\rho V/\eta = 0.024$. This value is much less than unity. In figure 2, we plot for the case of $V = 5$ m s^{-1} the continuum hydrodynamic prediction (equation (3)) versus distance to compare with the MD results. Obviously, the somewhat step-like features of the MD curves cannot be captured in the continuum model. This step-like structure indicates that water is squeezed-out in a layer-by-layer fashion. The dramatic increase in the normal force from MD simulation at $V = 5$ m s^{-1}, when compared with the continuum prediction for the same normal approach speed, suggests that this difference is related to the viscosity increase of the hydration water under subnanometer confinement. Very interestingly, if we consider the negative shift of the MD curve ($V = 5$ m s^{-1}) due to the initial attractive forces, we estimate that in the range 0.7–1.35 nm distances (2–4 hydration layers), the viscosity of hydration layers under such confinements is about 5–16 times the bulk value, which is somewhat less than what we have calculated previously [12] for an $H = 0.92$ nm hydration layer, and is in line with Raviv and Klein's SFB experimental results [7, 8], as well as the shear resonant measurement by Sakuma *et al* [26].

The fluidity of water under subnanometer confinement can also be understood from its diffusion and structure factor variations during the dynamic squeeze-out between two mica surfaces. Figure 7(A) shows the variation of the diffusion constant of confined water when the upper mica plate is held stationary at several distances. It is seen that in the 0.6–1.65 nm range the diffusion constants are well within two orders of magnitude of the bulk value ($D_{\rm bulk} = 3.31 \times 10^{-5}$ cm^2 s^{-1} for the TIP4P water model at 298 K) [27]. The density of confined water, however, is less than its bulk value due to the effects of hydration of interpolated K^+ ions and the hydrogen bonding between water molecules and mica surfaces. We have also calculated the variations of structure factor (the translational order parameter [16]), $\boldsymbol{q}(\boldsymbol{k})$, versus the distance during normal approach. The reciprocal lattice vector, $\boldsymbol{k}$, is defined based on the mica lattice unit cell. In figure 7(B), we see that q is below 0.15, indicating that the confined film is in a liquid phase. Further, the smooth decrease of water content in the mica slit pore suggests that the dynamic squeeze-out of water is a continuous process, and it appears that this process does not depend on the normal approach speed. To quantify how water molecules diffuse in different layers along the z-direction, we have also calculated the z-dependent diffusion constants of water using the bins method [28]. Figure 8 shows the diffusion distribution along the film thickness for a $H = 0.91$ nm hydration layer. Interestingly, the diffusion of water molecules near mica surfaces (in the adsorbed and the first hydration layer [23], see figure 5) is still significant, although decreased by roughly two orders of magnitude relative to the bulk value due to the hydrogen-bonding interactions between water molecules and mica surfaces. The diffusion of water

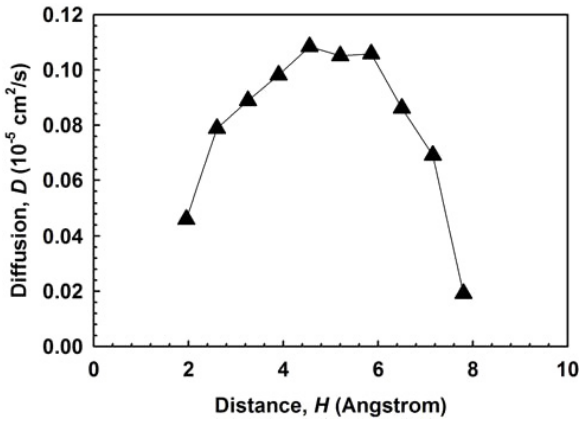

Figure 8. The diffusivity of water along the film thickness for an $H = 0.91$ nm three-layer hydration film.

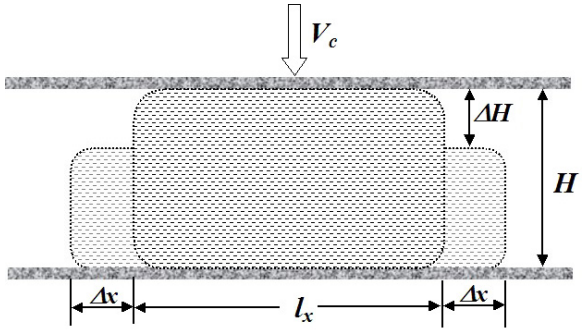

Figure 9. Schematic illustration of the steered diffusion of a water droplet under a critical normal approach speed, V_c.

Table 1. Critical normal approach speed in MD and surface force (SF) measurement regimes.

D (nm)	D_x (10^{-5} cm^2 s^{-1})	V_c (m s^{-1}) (MD) ($l_x = 4.15$ nm)	V_c (nm s^{-1}) (SF) ($l_x = 10$ μm)
1.65	1.312	4.78	823.1
1.35	0.822	1.86	319.6
0.91	0.199	0.16	27.82
0.60	0.014	0.003	0.536

molecules in the central region is about 3–5 times faster than that near the mica surface. The very fluidic nature of water in the central region indicates that the squeeze-out of water most likely starts from the central region. This is quite different from the scenario for non-polar liquids, in which the squeeze-out occurs at the first layer near the confining walls [10].

3.3. When will the measured hydration force be a real hydration force?—the steered diffusion model

Comparing figures 2 and 3 suggests that the *static relaxed* normal force in figure 3 is close to the back envelope of the force profiles in figure 2. This indicates that the static normal forces can be measured even though there is a finite normal approach speed, as long as this speed is less than some critical value. Indeed, this is usually a common practice in surface force measurements. We thus speculate if there exists a critical velocity, V_c, below which the real hydration force can be measured, and the hydrodynamic effects of confined water can be ruled out [29, 30]. In this scenario, the squeeze-out is dominated by the 'steered' diffusion of fluid molecules along the lateral direction. For nanoconfined hydration water, we note that in MD simulations this normal speed is still very much larger than those in surface force experiments. However, under the same degree of confinement, the diffusion dynamics of water molecules should remain the same regardless of the system size. Since the normal approach involves a 'layer-by-layer' squeeze-out of water molecules, intuitively, this would suggest that as the system size becomes larger, the time required to squeeze-out one layer of water molecules will become longer, and consequently, the critical normal approach speed should become slower. We now consider the 'steered diffusion' model as sketched in figure 9. When one-layer-thick hydration water, ΔH, is squeezed out, volume conservation requires that

$$l_x \Delta H = 2\Delta x (H - \Delta H). \tag{4}$$

The diffusion constant of water molecules along the x-direction can be approximately written as

$$D_x = \frac{\langle \Delta^2 x \rangle}{2t}, \tag{5}$$

which gives the free diffusion time t for Δx distance. From these two relations, the critical normal speed to squeeze out one layer of water molecules will be

$$V_c = \frac{\Delta H}{t} = 8\left(\frac{D_x}{\Delta H}\right)\left(\frac{H - \Delta H}{l_x}\right)^2. \tag{6}$$

We should emphasize that the above critical velocity, V_c, derived from this simple diffusion model may be an upper bound for the critical normal approach speeds, and there exists an alternative way to separate the hydrodynamic forces, as has been recently discussed by Challa and van Swol [31]. Now assuming $\Delta H = 0.25$ nm, the diameter of a water molecule, we have calculated from equation (6) the critical normal approach speed in the MD and surface force experimental regimes, respectively, as summarized in table 1. In column three, the MD simulations, we see that for $H = 1.65$ nm hydration water film, if the normal approach speed is greater than 4.78 m s^{-1}, hydrodynamic forces will begin to develop. The same is true for $D = 1.35$, 0.92, and 0.6 nm films for which the speed must be less than 1.86, 0.16, and 0.003 m s^{-1}, respectively, to eliminate any hydrodynamic effect. These are exactly what we have seen in figure 2, where the normal force profiles clearly show the commencement of hydrodynamic forces at different normal approach speeds and distances. The critical values of normal approach speed for a large contact area in surface force measurements (assuming the diameter of flattened area of mica is ca 10 μm) are shown in column four in table 1. These values decrease dramatically as the film thickness decreases. If a very large normal load is applied, leading to a larger flattened area, the normal approach speed should be very slow since it is inversely proportional to the squared contact diameter of the flattened area.

4. Conclusions

The normal forces between two mica surfaces in water and the dynamic squeeze-out behavior of water under nanometer confinement have been studied using molecular dynamics simulations. We use a liquid–vapor (L–V) molecular ensemble to properly represent the ambient condition in surface force experimental measurements. We find that repulsive hydration forces between mica surfaces in pure water will develop only at two-layer hydration water, corresponding to the occurrence of hydration shell overlaps between hydrated metal ions. The hydrodynamic pressure obtained from MD simulation has been compared to the continuum hydrodynamics prediction. We conclude that the fluidity of hydration water is maintained even during the squeeze-out of the last a few layers. The viscosity of hydration water under subnanometer confinement has been estimated as around 5–16 times the bulk value, consistent with recent viscosity measurements from different experimental groups. The present work also proposes a steered diffusion model for the prediction of critical normal approach speed, below which static hydration forces can be properly measured. However, this critical velocity may be the upper limit due to the simplicity of the model.

Acknowledgments

The author thanks Peter T Cummings and Jacob Klein for valuable discussion in this field. This work is supported by the National Science Foundation (NSF) CMMI-0700299, the US Department of Defense (DoD) Air Force Office of Scientific Research (AFOSR), and American Chemical Society (ACS) Petroleum Research Fund (PRF) 42935-AC9. The author also thanks significant computing allocation from the National Energy Research Scientific Computing Center (NERSC).

Appendix

In early MD simulations of the dynamic squeeze-out of water confined between two mica surfaces, we employed the NP_xT molecular ensemble in which the lateral pressure, p_x, was controlled by scaling x-coordinates of particles. The method of plane (MOP) [32] was used to calculate the lateral pressures, and the long-range contributions to these pressures from electrostatic interactions were calculated by the force-shifted method [33]. The Berendsen thermostat [34] was applied to the molecular system to control the temperature and pressure to the ambient condition. When the 1152-water droplet became quite elongated during squeeze-out, we found oscillatory waves in the lateral direction, exhibiting significant draw-in and squeeze-out of water molecules. This was later identified as an artifact of scaling the MD particle coordinates and box length in the x-direction, resulting in artificial oscillations in force profile. Figure A.1 shows such a force oscillation enhancement for the case of $V = 2$ m s^{-1}. The slight repulsive and oscillatory forces at larger distance came from the inaccurate pressure calculations, as well as the scaling effect. For comparison, the force profile obtained from L–V molecular ensemble at $V = 2.5$ m s^{-1} is also shown in the figure, which does not show the oscillatory behavior.

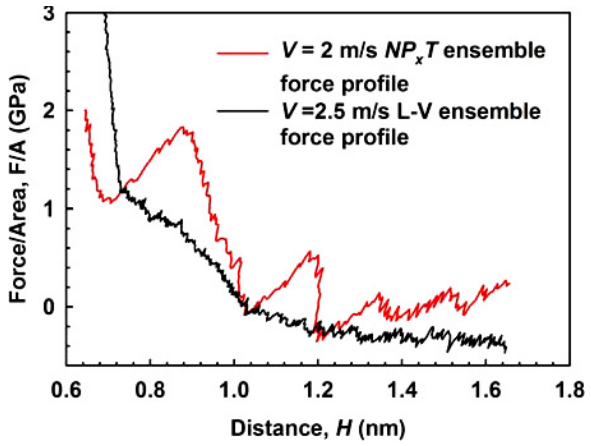

Figure A.1. Comparison of the variations of normal pressures derived from the NP_xT and L–V ensemble molecular dynamics simulations. The artificial force oscillation in NP_xT is due to the scaling of the MD particle coordinates and MD box length.

References

[1] Israelachvili J N 1991 *Intermolecular and Surface Forces* (New York: Academic)
[2] Derjaguin B V and Landau L 1941 *Acta Physicochim. URSS* **14** 633
[3] Verwey E J W and Overbeek J T G 1948 *Theory of the Stability of Lyophobic Colloids* (Amsterdam: Elsevier)
[4] Israelachvili J N and Adams G E 1978 *J. Chem. Soc. Faraday Trans.* I **74** 975
[5] Pashley R M 1981 *J. Colloid Interface Sci.* **80** 153
[6] Pashley R M 1981 *J. Colloid Interface Sci.* **83** 531
[7] Raviv U, Laurat P and Klein J 2001 *Nature* **413** 51
[8] Raviv U and Klein J 2002 *Science* **297** 1540
[9] Pashley R M and Israelachvili J N 1984 *J. Colloid Interface Sci.* **101** 511
[10] Persson B N J and Tosatti E 1994 *Phys. Rev.* B **50** 5590
[11] Persson B N J and Ballone P 2000 *J. Chem. Phys.* **112** 9524
[12] Leng Y S and Cummings P T 2005 *Phys. Rev. Lett.* **94** 26101
[13] Leng Y S and Cummings P T 2006 *J. Chem. Phys.* **125** 104701
[14] Koga K and Tanaka H 2005 *J. Chem. Phys.* **122** 104711
[15] Gao J P, Luedtke W D and Landman U 1997 *J. Chem. Phys.* **106** 4309
[16] Allen M P and Tildesley D J 1987 *Computer Simulation of Liquids* (Oxford: Clarendon)
[17] Vega C and de Miguel E 2007 *J. Chem. Phys.* **126** 154707
[18] Jorgensen W L *et al* 1983 *J. Chem. Phys.* **79** 926
[19] Odelius M, Bernasconi M and Parrinello M 1997 *Phys. Rev. Lett.* **78** 2855
[20] Boek E S, Coveney P V and Skipper N T 1995 *J. Am. Chem. Soc.* **117** 12608
[21] Lee S H and Rossky P J 1994 *J. Chem. Phys.* **100** 3334
[22] Klein J and Kumacheva E 1998 *J. Chem. Phys.* **108** 6996
[23] Cheng L *et al* 2001 *Phys. Rev. Lett.* **87** 156103
[24] Allen T Jr and Ditsworth R L 1972 *Fluid Mechanics* (New York: McGraw-Hill)
[25] Cameron A 1981 *Basic Lubrication Theory* (Chichester: Horwood)
[26] Sakuma H, Otsuki K and Kurihara K 2006 *Phys. Rev. Lett.* **96** 46104
[27] Mahoney M W and Jorgensen W L 2001 *J. Chem. Phys.* **114** 363
[28] Predota M *et al* 2004 *J. Phys. Chem.* B **108** 12049
[29] Israelachvili J, Maeda N and Akbulut M 2006 *Langmuir* **22** 2397

[30] Gourdon D and Israelachvili J 2006 *Phys. Rev. Lett.* **96** 99601
[31] Challa S R and van Swol F 2006 *Phys. Rev.* E **73** 16306
[32] Todd B D, Evans D J and Daivis P J 1995 *Phys. Rev.* E **52** 1627
[33] Beck D A C, Armen R S and Daggett V 2005 *Biochemistry* **44** 609
[34] Berendsen H J C *et al* 1984 *J. Chem. Phys.* **81** 3684